First-principles studies on clean and oxygen-adsorbed Ir(110) surfaces

P. Kaghazchi and T. Jacob*
Fritz-Haber-Institut der Max-Planck-Gesellschaft, Faradayweg 4-6, D-14195 Berlin, Germany
(Received 8 June 2007; revised manuscript received 22 September 2007; published 21 December 2007)

Using density functional theory in combination with an *ab initio* atomistic thermodynamics approach the structure and stability of Ir(110) surfaces in contact with an oxygen atmosphere have been studied. Besides the unreconstructed surface, (1×2)-, (1×3)-, and (1×4)-reconstructed Ir(110) have been considered. We find that without adsorption of oxygen all reconstructed surfaces are more stable than Ir(110)-(1×1). Adsorption of oxygen with coverages higher than 0.5 ML removes the surface reconstruction, leading to either a $c(2\times2)$ or $p(2\times1)$ oxygen overlayer on the unreconstructed Ir(110) surface and therefore an adsorbate-induced lifting of the reconstruction. While on almost all surfaces oxygen prefers binding at bridge positions to Ir atoms of the topmost layer, on the reconstructed surfaces higher coverages are required to additionally stabilize oxygen at adjacent threefold sites. Besides the stability of surface structures, our studies also reveal quantitative information on the geometry and energetics, providing further insights into the sometimes controversial discussion of oxygen adsorption on Ir(110).

DOI: 10.1103/PhysRevB.76.245425 PACS number(s): 68.43.Bc, 68.47.−b, 68.43.Fg, 71.15.Mb

I. INTRODUCTION

The structure of clean and oxygen-covered transition metal surfaces has been of great interest for many years. It was observed that some fcc(110) surfaces show strong reconstructions, leading to modified surface properties. While 3*d* and 4*d* metals, such as Cu(110), Ag(110), or Pd(110), preferentially reconstruct after adsorption of alkali metals (e.g., Na, K or Cs),[1–3] 5*d* metals, such as Au(110), Pt(110), or Ir(110), reconstruct already in their clean states.[4–10] In contrast to clean Au(110) and Pt(110) surfaces, which show a (1×2)-missing-row reconstruction,[11–17] the situation is more complex for Ir(110) and a variety of potential surface structures have been reported. Here the strong tendency towards stable {111} microfacets and nanofacets seems to be the driving force for different surface reconstructions, trying to minimize the overall surface free energy.[18,19]

The first experiments on clean Ir(110) using low-energy electron diffraction (LEED) proposed a (1×2)-missing-row structure similar to the one observed for Pt(110) and Au(110).[20–22] Further studies by time-of-flight scattering and recoiling spectrometry (TOF-SARS), ion scattering spectroscopy (ISS), and neutral impact collision ISS (NICISS) reported a (1×3) reconstruction, being characterized as two missing first-layer rows and one missing second-layer row in the center of each trough, mixed with (1×1) patches.[23–27]

Using auger-electron spectroscopy (AES) and reflection high-energy electron diffraction (RHEED) Hetterich *et al.*[28] showed that at room temperature the previously reported (1×2) reconstruction of Ir(110) could only be stabilized by Si impurities. However, these ion scattering experiments were not able to reveal the nature of the very complex LEED pattern on clean Ir(110) observed by several groups.[25,26] While the pattern was first discussed as some long-range ordering, more recent studies on Ir(110) combining helium atom diffraction, LEED, and STM[29–34] found that at room temperature mesoscopic ridges with (331) facets are present on the Ir(110) surface. Analyzing the STM images it was found that at about 500 K these (311) facets transform to a reconstructed (1×3)-missing-row surface structure interrupted by small (1×1) unreconstructed patches. At $T>800$ K the ridges finally disappear, leading to the already-mentioned (1×2)-missing-row reconstructed terraces.[32,34]

This was also supported by *in situ* LEED investigations, where at 890 K distinct (1×2) spots were observed instead of the streaky LEED patterns usually reported at room temperature. In order to explain this behavior, Schulz *et al.*[32] discussed this structural transformation of Ir to be a consequence of the temperature-dependent surface stress. Although in case of Pt(110) density-functional-theory (DFT) calculations indicated that the relief of surface stress might cause the (1×2) reconstruction,[35] DFT calculations by Filippetti and Fiorentini[36] showed that the stress-related concept should not be relevant for Ir(110). In their studies the tensile stress of the (1×2) reconstructed surface was even found to be larger than that of the unreconstructed surface. Furthermore, they calculated a 0.003 eV/Å^2 higher stability for the (1×2) reconstruction compared to the unreconstructed surface, showing that the energetics would already be sufficient to explain this transition. However, the calculated difference in surface energy is certainly within the overall DFT inaccuracy.

Besides the behavior of clean Ir(110), oxygen adsorption on this surface is considerably different compared to other transition metals and has been subject of intense studies.[20,21,25,27,30,37–40] While oxygen chemisorbs molecularly at low temperatures (<100 K), at higher temperatures only atomic oxygen has been found on the surface.[21] When clean Ir(110) is covered with oxygen to more than 0.25 monolayer (ML) at 300 K a $p(2\times2)$ LEED pattern is observed.[20,21,37] On the basis of contact potential difference (CPD) measurements the corresponding binding site was identified to be the bridge site on top of the rows.[21] Heating the thus-oxygen-covered surface to elevated temperatures (>700 K) at oxygen partial pressures of 5×10^{-8} mbar causes significant modifications on the surface structure, being subject of controversial discussion. Although almost all experimental work agrees that at higher temperatures oxygen

is somewhat randomly distributed on the surface and stabilizes the structure of an unreconstructed Ir(110)-(1×1), the question about the exact location of the oxygens remains unanswered and has established the expression "oxidized surface." While some groups proposed the formation of a surface oxide,[21,37] in which the oxygen atoms occupy subsurface positions, leaving the regular structure of the Ir substrate almost undisturbed, others do not support this picture but assume an adsorbate layer.[25,27,30,38–40] For both cases the nature of the (sub)surface oxygen is quite different from the corresponding IrO_2 bulk oxide.[41] For instance, the latter one decomposes already at around 540 K, while the surface oxide requires temperatures around 850–900 K at $p_{O_2}=1\times10^{-11}$ atm.[41]

By varying the further treatment of this oxygen-containing (0.25 ML) unreconstructed Ir(110)-(1×1) surface, different structures have been prepared. Using LEED, Taylor *et al.*[21] observed a (1×4) pattern after heating to more than 1200 K and proposed an ordered distribution of oxygens residing below the surface on the bridging sites between two atoms in adjacent rows. However, keeping the surface at room temperature and adsorbing an additional 0.5 ML of oxygen results in a $c(2\times2)$ LEED pattern where the adsorbates are located at bridge sites on top of the rows.[21,25,37–39] Due to the discrepancy between the total oxygen exposure of 0.75 ML and the 0.5 ML being connected with the observed $c(2\times2)$ pattern, Taylor *et al.*[21] assumed that the first 0.25 ML occupied subsurface positions. This would finally support the picture of an initial surface oxide.

Motivated by the variety of different experiments on clean and oxygen-containing Ir(110), we present in this paper theoretical calculations on unreconstructed and reconstructed Ir(110) surfaces using DFT together with thermodynamic considerations. In Sec. II we will briefly describe our DFT calculations and the *ab initio* atomistic thermodynamics method.[42–45] Our results on the clean and oxygen-covered surfaces of unreconstructed and reconstructed Ir(110) are described in Sec. III, allowing us to draw the corresponding surface phase diagram (Sec. IV). Finally, a summary as well as outline directions for future work will be given in Sec. V.

II. METHOD

A. DFT calculations

Density functional theory slab calculations were performed using the CASTEP code.[46] For all atoms the core electrons were replaced by Vanderbilt ultrasoft pseudopotentials,[47] and the exchange-correlation energies were evaluated with the Perdew-Burke-Ernzerhof (PBE) form of the generalized gradient approximation (GGA).[48] The different surfaces were modeled with layer-converged supercells consisting of 12-layer slabs for unreconstructed and (1×2) reconstructed Ir(110) and 13-layer slabs for (1×3) and (1×4) reconstructed Ir(110). Periodically repeated slabs were separated by a ≈12 Å vacuum to decouple the interactions between neighboring slabs in the supercell geometry. For each system, the bottom four layers were fixed at the calculated bulk crystal structure and the remaining surface layers and the adsorbates were allowed to freely relax (to <0.01 eV/Å). The Brillouin zones of the (1×1)-surface unit cells of Ir(110)-(1×1), -(1×2), -(1×3), and -(1×4) were sampled with converged $10\times14\times1$, $5\times14\times1$, $3\times14\times1$, and $2\times14\times1$ Monkhorst-Pack k-point meshes, respectively. As basis set an energy cutoff of 340 eV was used, which by performing spin-polarized calculations led to a bond length and dissociation energy of molecular O_2 of 1.23 Å and 5.60 eV. Throughout the paper binding energies are with respect to half a gas-phase O_2 molecule.

An extensive and careful analysis of the error sources that are related to slab thickness, vacuum size, plane-wave cutoff, and k-point mesh shows that when using the values given above the overall error bar in the surface free energy is $\sim4-5$ meV/Å^2. Furthermore, in order to give an estimate of the inaccuracies coming from the use of pseudopotentials, we also calculated the difference in the surface free energy for oxygen at two different binding sites with a full-potential (all-electron) approach (using the WIEN2K code[49]). Comparison shows a difference of only ~0.4 meV/Å^2 in the surface free energy.

Finally, we also checked for inaccuracies coming from the use of different surface unit cells and slab thicknesses. For the clean Ir(110)-$(1\times n)$, $n=1,2,3$, surfaces we evaluated the surface free energies with the same (1×6) unit cell, having an identical number of layers, k-point vacuum size, and energy cutoff. In each case the difference from the surface free energy calculated with the models described above was found to be less than 0.5 meV/Å^2.

B. Thermodynamical considerations

To evaluate the (p,T)-surface phase diagram from first principles, we use DFT electronic structure calculations together with the *ab initio* atomistic thermodynamics approach.[42–45] Since the stability of a particular surface structure is given by its surface free energy, the most stable surface composition and geometry for a specific orientation is the one that minimizes the surface free energy given as

$$\gamma(T,\{p_i\},\{N_i\})=\frac{1}{A}\left[G(T,\{p_i\},\{N_i\})-\sum_i N_i\mu_i(T,p_i)\right], \quad (1)$$

where G is the Gibbs free energy of the system (in practical calculations the energy of the slab), A is the surface area, and μ_i is the chemical potential of the N_i atoms of species i the system is in contact with. In the present work the Ir(110) surface is considered to be in thermodynamic equilibrium with two reservoirs: Ir bulk and an O_2 atmosphere. Therefore, assuming the temperature and pressure dependence of the solid phases to be small, Eq. (1) becomes

$$\gamma(T,p_{O_2},N_{Ir},N_O)=\frac{1}{A}[G(T,p_{O_2},N_{Ir},N_O)-N_{Ir}\mu_{Ir}^{bulk}-N_O\mu_O(T,p_{O_2})]. \quad (2)$$

In Eq. (2) the Gibbs free energy G of the surface (slab) as well as the oxygen chemical potential have contributions

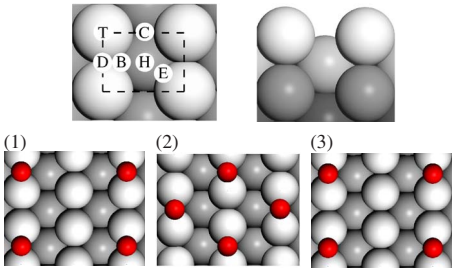

FIG. 1. (Color online) Top and side view of Ir(110)-(1×1) showing all binding sites at which O adsorption has been considered (top), as well as the most stable structures for the different coverages (bottom).

from the internal energy U, which we take as the DFT-calculated total energy, configurational entropy, and vibrational free energy F^{vib}.

The last term on the right-hand side of Eq. (2) includes the main temperature and pressure dependence through the chemical potential of the oxygen-reservoir:

$$\mu_{\mathrm{O}}(T,p_{\mathrm{O}_2}) = \frac{1}{2}\left[E^{\mathrm{tot}}_{\mathrm{O}_2} + \bar{\mu}_{\mathrm{O}_2}(T,p^0) + k_{\mathrm{B}}T\ln\left(\frac{p_{\mathrm{O}_2}}{p^0}\right)\right]. \quad (3)$$

Here $E^{\mathrm{tot}}_{\mathrm{O}_2}$ is the DFT-calculated total energy of an isolated O_2 molecule and $\bar{\mu}_{\mathrm{O}_2}(T,p^0)$ is the standard chemical potential that includes all contributions from vibrations and rotations of the molecule and the ideal gas entropy at 1 atm. Although the standard chemical potentials can be calculated from first principles, we use the corresponding $\bar{\mu}_{\mathrm{O}_2}(T,p^0)$ values from the JANAF thermodynamic tables.[51]

Since in the present work we are only interested in relative stabilities of different adsorbate phases, it is reasonable to neglect contributions from configurational entropy.[45] The vibrational contributions to γ coming from oxygen can be estimated by[50]

$$\gamma^{\mathrm{vib}}(T) \sim \frac{1}{A}\left[\sum_i^{N_{\mathrm{O}}} F_i^{\mathrm{vib}}(T,\omega_i^{\mathrm{surf}}) - N_{\mathrm{O}}F^{\mathrm{vib}}(T,\omega^{\mathrm{gas}}_{\mathrm{O}_2})\right], \quad (4)$$

with

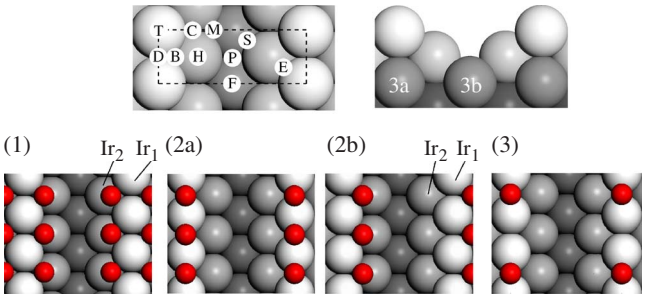

FIG. 2. (Color online) Top and side view of Ir(110)-(1×2) showing all binding sites at which O adsorption has been considered (top), as well as the most stable structures for the different coverages (bottom).

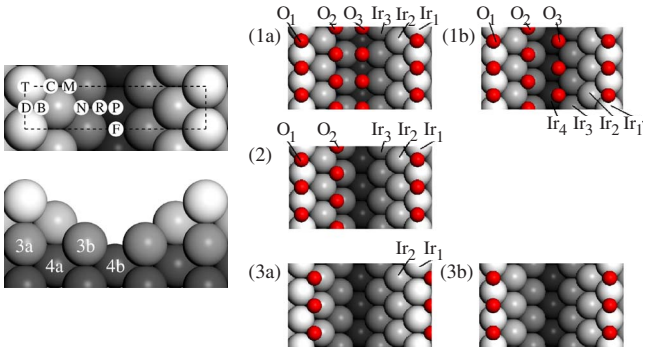

FIG. 3. (Color online) Top and side view of Ir(110)-(1×3) showing all binding sites at which O adsorption has been considered (left), as well as the most stable structures for the different coverages (right).

$$F^{\mathrm{vib}}(T,\omega) = \frac{1}{2}\hbar\omega + k_{\mathrm{B}}T\ln(1-e^{-\hbar\omega/k_{\mathrm{B}}T}). \quad (5)$$

In Eq. (4), ω_i^{surf} is the O-surface stretch frequency of the ith adsorbed oxygen in the corresponding configuration and $\omega^{\mathrm{gas}}_{\mathrm{O}_2}$ is for the O_2 molecule in the gas phase. At typical experimental pressures of 5×10^{-11} atm and temperatures at which phase transitions are expected (<1200 K), we estimated these contributions to be rather small, leading to a slight temperature shift of <20 K only, but not causing any modifications in the ordering of surface phases. Therefore, in the present work vibrational contributions have not been considered.

III. RESULTS AND DISCUSSION

On the basis of the calculated lattice constant of 3.90 Å (expt.:[52] 3.84 Å) we modeled unreconstructed Ir(110)-(1×1) as well as reconstructed Ir(110)-(1×2), -(1×3), and -(1×4) as shown in Figs. 1–4. The surface free energies calculated for the clean surfaces (see Table I) show that the reconstructed surfaces are more stable than Ir(110)-(1×1) by 5–8 meV/Å^2. Even when considering the overall error in

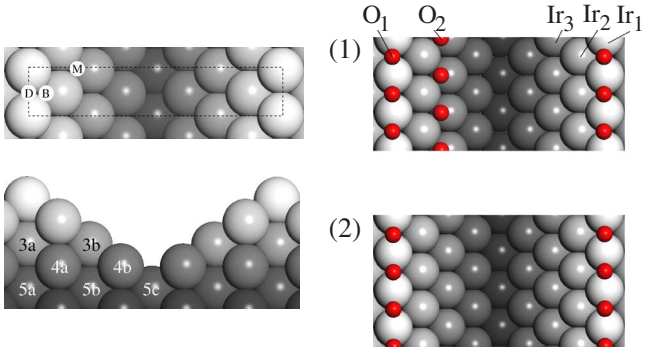

FIG. 4. (Color online) Top and side view of Ir(110)-(1×4) showing all binding sites at which O adsorption has been considered (left), as well as the most stable structures for the different coverages (right).

TABLE I. Surface free energies γ and relaxations of the clean unreconstructed and reconstructed surfaces. Δd_{ij} denotes the change in the distance between layers i and j (averaged over all atoms in the same layer), given as precentage of the bulk interlayer spacing. The buckling within each layer is given by Δz (for labels see Figs. 1–4), again as precentage of the bulk interlayer spacing.

Structure	γ [eV/Å^2]	Δd_{12}	Δd_{23}	Δd_{34}	Δd_{45}	Δz_{3a}	Δz_{3b}	Δz_{4a}	Δz_{4b}	Δz_{5a}	Δz_{5b}	Δz_{5c}
Unreconst. (1×1)	0.192	−12.2	5.4	−0.3	−1.0							
Reconst. (1×2)	0.187	−8.6	−3.6	1.0	−0.7	−5.1	5.1					
Reconst. (1×3)	0.185	−8.4	−1.7	−3.0	0.4	−2.0	1.0	−3.5	7.0			
Reconst. (1×4)	0.184	−8.0	−1.8	−1.7	−2.8	−1.4	0.7	−1.3	1.3	−2.4	−2.3	7.0

the surface free energy of ~4–5 meV/Å^2 (see Sec. II A), our calculations still indicate a preference for reconstruction, which is in agreement with experiments.[4–10,32,34] In these experiments it was also observed that at elevated temperatures and an oxygen partial pressure of 5×10^{-11} atm there is coexistence of different reconstructed surfaces. This is also supported by our calculations, since the stability of the three reconstructed surfaces differs only by 1–3 meV/Å^2, which is within the inaccuracy of the calculations.

Regarding the surface structure of unreconstructed Ir(110), we obtain the characteristic behavior of fcc(110) surfaces (see Ref. 53 and references therein), showing a strong contraction of the outermost layer separation (−12.2%), followed by a damped oscillatory relaxation behavior of the inner layers (+5.4,−0.3%). Since the reconstructed surfaces are more open, giving the inner layer atoms more flexibility in occupying there optimal positions, the relaxation is modified compared to Ir(110)-(1×1). First, the outermost layers are less contracted (between −8.0 and −8.6%), and second, the damped oscillatory relaxation behavior is only observed after a full layer of atoms is formed. Consequently, the two topmost layers of Ir(110)-(1×2), the three topmost layers of Ir(110)-(1×3), and the four topmost layers of Ir(110)-(1×4) are all contracted compared to the bulk layer spacing. This in conformity with the buckling within each layer, for which we find strong effects in the first full atom layer of each system. For example, the two distinct atoms in the third layer of Ir(110)-(1×2) have z coordinates different by 0.14 Å (or 2×5.1 % of the bulk layer spacing).

After the clean surfaces, the adsorption of atomic oxygen has been studied for different coverages Θ, which for all surfaces is with respect to the same surface area (see Figs. 1–4): $\Theta=0.25$, 0.5, and 1 ML for O/Ir(110)-(1×1) and O/Ir(110)-(1×2); $\Theta=1/3$, 2/3, and 1 ML for O/Ir(110)-(1×3); $\Theta=0.25$ and 0.5 ML for O/Ir(110)-(1×4). Figures 1–4 show the different higher-symmetric binding sites at which oxygen binding has been studied (left figures) as well as optimized structures of the most stable configurations for each coverage considered. The corresponding binding energies per oxygen, Ir-O bond lengths, and interlaying spacings of the substrate are summarized in Table II.

A. Oxygen on Ir(110)-(1×1)

On the unreconstructed surface several ordered oxygen structures were considered for each coverage. While at 0.25 ML we focused on $p(2\times2)$- and $p(1\times4)$-O, at 0.5 ML $p(1\times2)$-, $p(2\times1)$-, and $c(2\times2)$-O adlayers have been studied. We find that for all coverages the bridge site (D site) is preferred (see Fig. 1).

At 0.25 ML only weak lateral adatom interactions can be expected. Therefore, the binding energy of 2.04 eV and bond length of d(Ir-O)=1.97 Å we calculate for a $p(2\times2)$-O adlayer at the D site should almost represent the zero-coverage limit. As a consequence of the strong interaction between oxygen and the surface, both Ir atoms to which the adatom binds are displaced by 0.07 Å away from the oxygen. This behavior, which seems to be more general for the late $5d$ elements, is also known as *row pairing*. Significantly lower binding energies were obtained for C ($E_{\mathrm{bind}}=1.24$ eV), B ($E_{\mathrm{bind}}=1.22$ eV), and T sites ($E_{\mathrm{bind}}=1.16$ eV). We also considered the $p(1\times4)$-O structure proposed by Taylor *et al.*,[21] in which the adatoms occupy subsurface C sites. However, we find this configuration to be unstable. After geometry optimization the final position is still the C site, but it is now 1.1 Å above the Ir surface ($E_{\mathrm{bind}}=1.32$ eV). Keeping the $p(1\times4)$ structure, we also checked for oxygen at on-surface D sites, for which we found a 0.18 eV higher binding energy, which is still less than the $p(2\times2)$ adlayer.

At 0.5 ML $c(2\times2)$- and $p(2\times1)$-O are both more stable than the $p(1\times2)$-O adlayer with binding energies per oxygen of 2.09 and 2.04 eV, respectively (oxygen at D sites). The geometry of the most stable configuration [$c(2\times2)$-O] shows good agreement with experimental measurements on the "oxidized" surface.[39] For the Ir-O distance and the vertical separation of the topmost substrate layers we calculate values of d(Ir-O)=1.97 Å and $d_{12}=1.31$ Å, which should be compared to the corresponding experimental distances of 1.93±0.07 Å and 1.33±0.07 Å. This agreement is rather interesting, since the experimentally prepared $c(2\times2)$-O structure is usually thought of being adsorbed on an already formed surface oxide,[21,25,37–39] while in our calculations we assume a pure Ir(110)-(1×1) surface.

At a coverage of 1 ML the D site still remains energetically favored with binding characteristics of $E_{\mathrm{bind}}=1.59$ eV and d(Ir-O)=1.99 Å. Interestingly, the top site (T site) becomes the second favorable adsorption site ($E_{\mathrm{bind}}=1.10$ eV). Whereas at D sites the Ir-O bond length is almost independent of the coverage, the adsorbates are closer to the surface plane by ~0.06 Å for both 0.25 ML and 0.5 ML compared to 1 ML. In addition the calculated binding energy is significantly lower for 1 ML than for 0.25 and 0.5 ML by 0.45 and 0.50 eV, which is a direct consequence of a strong O-O repulsion.

TABLE II. Calculated binding energies (referenced to 1/2 O_2) and bond lengths (as labeled in Figs. 1–4) for oxygen on Ir(110) surfaces at different coverages. Only the most stable structure for each coverage is listed. Similar to Table I, Δd_{ij} is the change in the distance between Ir-substrate layers i and j (averaged over all atoms in the same layer), given as precentage of the bulk interlayer spacing.

Structure	Coverage [ML]	E_{bind} [eV] (per 1/2 O_2)	Distances [Å]	Δd_{12}	Δd_{23}	Δd_{34}	Δd_{45}
Unreconst. (1×1)	1.0	1.59	Ir-O=1.99	0.4	−3.2	4.0	−0.3
	0.5	2.09	Ir-O=1.97	−4.9	1.2	1.2	−1.6
	0.25	2.04	Ir-O=1.97	−8.0	2.6	0.5	−1.4
Reconst. (1×2)	1.0	1.34	Ir_1-O=2.08	6.9	−1.8	−1.5	1.8
			Ir_2-O=2.07				
[see Fig. 2(2a)]	0.5	1.61	Ir-O=1.99	1.4	−7.1	3.3	0.0
[see Fig. 2(2b)]	0.5	1.61	Ir_1-O=2.08	−3.5	−2.6	−0.2	1.0
			Ir_2-O=2.10				
	0.25	2.07	Ir-O=1.98	−2.7	−4.6	2.2	−0.3
Reconst. (1×3)							
[see Fig. 3(1a)]	1.0	1.21	Ir_1-O_1=1.99	0.0	−7.6	6.0	−2.8
			Ir_3-O_2=2.12				
			Ir_2-O_2=2.06				
			Ir_3-O_3=1.99				
[see Fig. 3(1b)]	1.0	1.22	Ir_1-O_1=2.00	1.9	−0.9	1.1	0.3
			Ir_2-O_2=2.08				
			Ir_3-O_2=2.09				
			Ir_3-O_3=2.07				
			Ir_4-O_3=2.12				
	2/3	1.48	Ir_1-O_1=2.00	0.1	−2.1	−0.8	−0.4
			Ir_2-O_2=2.09				
			Ir_3-O_2=2.08				
[see Fig. 3(3a)]	1/3	1.63	Ir_1-O_1=2.08	−4.1	−1.1	−4.6	1.5
			Ir_2-O_1=2.10				
[see Fig. 3(3b)]	1/3	1.62	Ir_1-O_1=1.99	1.3	−4.7	−2.2	1.1
Reconst. (1×4)	0.5	1.48	Ir_1-O_1=1.99	1.1	−2.5	0.5	−3.0
			Ir_2-O_2=2.09				
			Ir_3-O_2=2.08				
	0.25	1.60	Ir-O=1.99	1.9	−4.7	−0.6	−2.1

Regarding the changes in surface relaxation we find a significant correlation with oxygen coverage, which can be explained by the strong interaction between adsorbate and substrate. While without oxygen the spacing between the topmost surface layers was contracted by −12.2% (compared to the bulk), successive adsorption of oxygen reduces this contraction until there is even a slight expansion of +0.4% at $\Theta=1$ ML. The changes in the topmost layer also influence the underlying substrate layers such that the damped oscillatory relaxation behavior, which was found for the clean substrate, is disturbed with increasing oxygen adsorption and even reversed in case of 1 ML coverage.

B. Oxygen on Ir(110)-(1×2)

Similar to the unreconstructed surface, 0.25, 0.5, and 1 ML coverages have been considered with Ir(110)-(1×2). Having 0.25 ML oxygen adsorbed in a $p(2\times2)$-O configuration (D sites) results in a binding energy of 2.07 eV, which is almost the value obtained for $p(2\times2)$-O on the unreconstructed surface. This suggests that removing a row of topmost Ir atoms has minor effects on the oxygen binding.

At 0.5 ML we find that besides the D site, binding at the higher-coordinated B site (hollow position) gives the same adsorption energy of 1.61 eV. This is different compared to the 1 ML system, where both oxygens of the unitcell occupy B sites [see Fig. 2(1)]. Although oxygen might still prefer binding at D sites, at this coverage half of the oxygens would have to occupy lower-lying surface sites (e.g., M or P sites), at which binding is significantly less stable. As a consequence the system with O atoms at D and M sites is 0.17 eV per oxygen less stable than having both oxygens at B sites.

As was found for the unreconstructed surface, the strong oxygen-substrate interaction weakens the connections be-

tween Ir atoms to which oxygens bind and the remaining substrate, causing an increase in the layer spacing. This effect becomes more pronounced at higher oxygen coverages. Since at 1 ML two oxygens are bound at *B* sites, Δd_{12}, which was −8.6% before adsorption, increases to +6.9%.

C. Oxygen on Ir(110)-(1×3)

Due to the periodicity of (1×3)-reconstructed Ir(110), coverages of 1/3, 2/3, and 1 ML have been considered. Similar to the Ir(110)-(1×2) reconstructed surface, again oxygen prefers both *D* sites (E_{bind}=1.62 eV) and *B* sites (E_{bind}=1.63 eV) for 1/3 ML [see Figs. 3(a) and 3(b)]. While these binding energies are significantly lower (by 0.44 eV) compared to the 0.25 ML coverage case on Ir(110)-(1×2), the Ir-O bond length increases only slightly by 0.01 Å. However, both the Ir-O bond lengths and binding energies at *D* and *B* sites are comparable to the 0.5 ML coverage case on Ir(110)-(1×2) (see Table II). The next stable surface sites on Ir(110)-(1×3) are the *M* (E_{bind}=1.30 eV) and *C* sites (E_{bind}=1.22 eV), which are both threefold hollow positions. Interestingly, we calculate the lowest adsorption energy for the *P* site (E_{bind}=0.28 eV), which is the lowest accessible position below the surface plane (see Fig. 3).

For two oxygen atoms per Ir(110)-(1×3) unit cell (2/3 ML) we find that a structure where *D* and *M* sites [see Fig. 3(2)] are occupied is most stable (E_{bind}=1.48 eV). Although from the relatively strong O-O repulsion one would expect an adlayer configuration in which the spacing between the oxygens is maximized (i.e., *D* and *P*/*F* sites), the stronger binding at *M* sites compared to *P* or *F* sites (ΔE_{bind}=0.56 eV and ΔE_{bind}=0.29 eV) stabilizes this configuration.

Adding a third oxygen atom to the Ir-(1×3) unit cell, resulting in 1 ML, stabilizes the two different configurations shown in Fig. 3(1a) (E_{bind}=1.21 eV) and Fig. 3(1b) (E_{bind}=1.22 eV). Apparently occupation of either *F* or *R* sites (besides already occupied *D* and *M* sites) results in almost the same binding energy of 1.22, and 1.21 eV, respectively. Thus, the stronger O-O repulsion, which we expect for the system 3(1a), seems to have minor impact. Interestingly, the structure in which the three oxygen atoms per unit cell are distributed more homogeneously was found to be even slightly less stable: O atoms at *D*, *N*, and *N* sites (E_{bind}=1.18 eV).

D. Oxygen on Ir(110)-(1×4)

For the (1×4)-reconstructed Ir(110) surface only selected surface sites and coverages (Θ=0.25 and 0.5 ML) have been considered. This restriction is motivated by the results we have already obtained for the previous systems, but also by the rather extended unit cell size. Although certainly of interest, we find that higher-coverage phases are of minor relevance for the surface phase diagram that will be discussed in the next section.

Similar to the other surfaces, a single oxygen atom per unitcell again prefers the *D* site with a binding energy of 1.60 eV. As almost the same binding energy of 1.62 eV was obtained for the $p(1\times3)$ adlayer on Ir(110)-(1×3), we conclude there are only minor O-O interactions along the direction of reconstruction.

Regarding the 0.5 ML, we studied two configurations only. The first with both oxygens at *B* sites, which can be compared to 1 ML on Ir(110)-(1×2), and the second with oxygens at *D* and *M* sites, similar to 2/3 ML on Ir(110)-(1×3). Among these two systems, we find the latter one to be more stable, giving a binding energy of 1.48 eV, which is exactly the value we had obtained for 2/3 ML oxygen on Ir(110)-(1×3). This again confirms the conclusion on the weak O-O interaction along the direction of reconstruction drawn above.

By comparing the results for oxygen adsorption at different coverages, we see similar binding energies for oxygen at *D* sites for one oxygen atom per reconstructed Ir(110)-(1×*n*), $n=1,\ldots,4$, unit cells. As expected, the binding energy at the most stable position (mostly *D* site) increases significantly from 1 ML over 0.5–0.25 ML on the unreconstructed substrate. However, at low coverages keeping the adlayer structure but removing entire atomic surface rows raises the binding energy only slightly.

Regarding the binding sites we find that on the unreconstructed substrate the bridge position is most stable at all coverages (*D* site), but on the reconstructed surfaces threefold-coordinated sites become additionally stabilized.

Due to a relatively strong interactions between adsorbates and substrate, a modified relaxation behavior of the surfaces can be observed compared to the clean surfaces. These Ir atoms to which oxygens are bound weaken their connection to the underlying substrate, leading to an increase of the corresponding layer spacings. This in turn has direct consequences for the spacings between the other surface near layers.

IV. SURFACE PHASE DIAGRAM OF O/Ir(110)

In order to evaluate the stability of surface structures as a function of temperature and partial pressure of the surrounding oxygen atmosphere, we employed the *ab initio* atomistic thermodynamics approach as described in Sec. II B. By using Eq. (2) together with the DFT-calculated total energies, we obtained the surface phase diagram shown in Fig. 5. Each individual line corresponds to one of the clean or oxygen-covered Ir(110) surfaces discussed before. Since our focus is on oxygen adsorption on pure Ir, the phase diagram is valid in the oxygen chemical potential range, where the bulk oxide, having a rutile-type structure, is not stable (see Fig. 5).

Using our calculational parameters we evaluate the heat of formation for Ir bulk oxide (IrO_2) to be $\Delta\mu_O$=0.93 eV per oxygen, while the experimental value[54] is ΔH_f^0=1.17 eV/O. Since this discrepancy is related to the known difficulties in describing the O_2 molecule within DFT, we adjusted our phase diagram to reproduce the experimental value. This means a modified reference for the oxygen chemical potential has been used.

The finally obtained surface phase diagram shows that at low oxygen chemical potentials the clean reconstructed Ir(110)-(1×3) and Ir(110)-(1×4) surfaces, represented by a

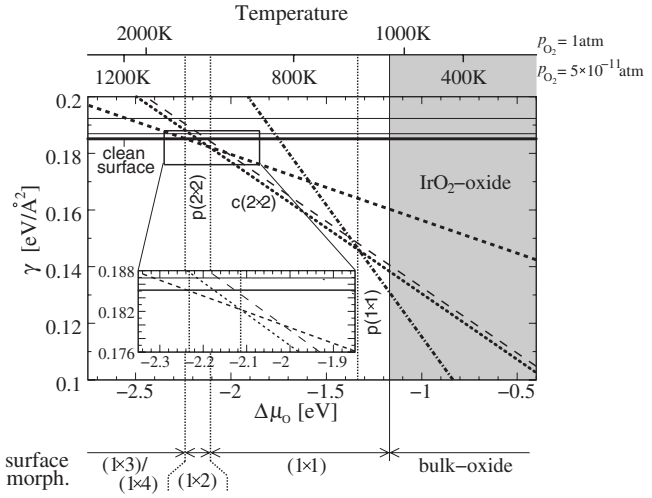

FIG. 5. Calculated surface phase diagram showing γ as function of $\Delta\mu_O$, which is defined as $\Delta\mu_O=\mu_O-\frac{1}{2}E^{tot}_{O_2}$. The dependence on the oxygen chemical potential is converted to temperature scales at pressures of 1 atm and 5×10^{-11} atm. While the adlayer structure is given as label to each line, the corresponding surface morphology is indicated below the diagram with $(1\times n)$ meaning the Ir(110)-$(1\times n)$ surface.

single low-lying horizontal line, have the lowest surface free energies and thus are thermodynamically most stable. While the surface free energy of clean reconstructed Ir(110)-(1×2) is only 2–3 meV/Å^2 higher, unreconstructed Ir(110)-(1×1) is significantly less stable (by $\approx$8 meV/Å^2), even when considering the overall accuracy of the calculations.

Lowering the temperature or increasing the oxygen partial pressure results in the formation of a $p(2\times2)$-O adlayer on Ir(110)-(1×2) between $\Delta\mu_O=-2.24$ and -2.12 eV. At the upper end of this chemical potential range, we find that there is a transition to the $c(2\times2)$-O or $p(2\times1)$-O adlayer on unreconstructed Ir(110)-(1×1), which are the thermodynamic stable configurations up to $\Delta\mu_O=-1.34$ eV. Despite the slight preference for the $c(2\times2)$-O over the $p(2\times1)$-O structure (see Fig. 5), here we mention both because the difference is certainly within the accuracy of our calculations. Although the $p(1\times2)$-O structure on the unreconstructed surface has the same coverage as the $p(2\times1)$-O adlayer, the ability of the latter one for row-pairing Ir atoms results in a higher stability of $\Delta\gamma=0.020$ eV/Å^2. Further increase of the oxygen chemical potential does not change the preferred substrate structure but increases the coverage of the adlayer to 1 ML in a $p(1\times1)$ configuration. Finally the oxygen-rich limit corresponds to the oxygen chemical potential of IrO_2 bulk-oxide formation, which is reached at the experimental value of $\Delta\mu_O=-1.17$ eV that had been used as calibration. The surface phase diagram makes also apparent that none of the oxygen adlayers on reconstructed Ir(110)-(1×3) and Ir(110)-(1×4) are favorable at any oxygen chemical potential.

In order to allow for a better comparison with experiment, we used Eq. (3) to convert the oxygen chemical potential $\Delta\mu_O$ to temperature scales for specific partial pressures. In Fig. 5 temperature scales for $p_{O_2}=1$ atm and 5×10^{-11} atm are shown. Since many experiments were performed under the latter pressure condition, it will be the basis for the remaining discussion. The $p(2\times2)$-O structure has been observed experimentally after exposing 0.25 ML oxygen on clean Ir(110) at room temperature, which according to our phase diagram should be (1×2) reconstructed. Our calculations show that the $p(2\times2)$-O configuration on Ir(110)-(1×2) is the thermodynamically most stable structure between 990 and 1050 K. Considering only 0.25 ML coverages this configuration remains stable over the entire temperature range, from 575 K where IrO_2 bulk oxide decomposes until complete oxygen desorption at around 1050 K.

Besides the (1×4)-subsurface pattern proposed by Taylor *et al.*,[21] which we found to be not stable, we have not considered other surface-oxide structures. Therefore, we are so far not able to contribute to the discussion, which structure is formed when heating the 0.25 ML oxygen-covered surface to elevated temperatures. Instead we find the $c(2\times2)$-O overlayer, which is experimentally formed by exposing 0.5 ML oxygen on the already oxygen-containing (0.25 ML) surface at room temperature (giving an overall coverage of 0.75 ML), to be thermodynamically most stable between approximately 990 K and 650 K. The latter value is again the temperature where the $p(1\times1)$-O phase starts to form. Interestingly, the geometry of the $c(2\times2)$-O adlayer we studied on pure unreconstructed Ir(110)-(1×1), nicely compares to the experimental measurements (see Sec. III), which in parts assume a surface oxide as substrate.

Finally for temperatures lower than 575 K the IrO_2 bulk oxide becomes thermodynamically stable.[41]

V. SUMMARY AND OUTLOOK

In this paper we investigated clean and oxygen-covered surfaces of unreconstructed and reconstructed Ir(110) by DFT together with thermodynamic considerations, providing detailed information on the structure and energetics of a variety of oxygen coverages. It has been shown that without oxygen adsorption Ir(110) prefers to reconstruct in a $(1\times n)$, $n=2,3,4$, missing-row structure. While Ir(110)-(1×3) and Ir(110)-(1×4) show almost the same stability, the difference in surface free energy of Ir(110)-(1×2) is within the inaccuracy of the calculations. This is in agreement with experiments, which observed the coexistence of these structures on clean Ir(110).

Adsorption of oxygen first leads to a $p(2\times2)$-O adlayer adsorbed on still reconstructed Ir(110)-(1×2) and reaching a coverage of 0.5 ML the reconstruction of Ir(110) is finally lifted. At this coverage we find a $c(2\times2)$-O adlayer on Ir(110)-(1×1), but $p(2\times1)$-O shows a comparable stability. The former structure has also been observed by several experimental groups after depositing 0.5 ML oxygen on the already 0.25-ML-covered surface. Therefore, further studies will aim at a better understanding of the morphology and role of a potential surface oxide.

Finally from our calculations we were also able to identify the favorable adsorption sites for structures observed by experiments. On all four Ir(110) surfaces oxygen prefers binding at bridge positions on the rows formed by Ir atoms. In addition, on the reconstructed surfaces threefold sites located next to the rows are also stabilized in the case of higher oxygen coverages.

ACKNOWLEDGMENTS

The authors gratefully acknowledge support from the German Academic Exchange Service (DAAD), the "Fonds der Chemischen Industrie" (FCI), and the "Deutsche Forschungsgemeinschaft" (DFG) within the Emmy-Noether-Program.

*jacob@fhi-berlin.mpg.de

[1] B. E. Hayden, K. C. Prince, P. J. Davies, G. Paolucci, and A. M. Bradshaw, Solid State Commun. **48**, 325 (1983).
[2] R. Schuster, J. V. Barth, G. Ertl, and R. J. Behm, Surf. Sci. Lett. **247**, L229 (1991).
[3] C. J. Barnes, M. Q. Ding, M. Lindroos, R. D. Diehl, and D. A. King, Surf. Sci. **162**, 59 (1985).
[4] W. Moritz and D. Wolf, Surf. Sci. Lett. **88**, L29 (1979).
[5] W. Moritz and D. Wolf, Surf. Sci. Lett. **163**, L655 (1985).
[6] J. Möller, H. Niehus, and W. Heiland, Surf. Sci. **166**, L111 (1986).
[7] K. M. Ho and K. P. Bohnen, Phys. Rev. Lett. **59**, 1833 (1987).
[8] M. Copel and T. Gustafsson, Phys. Rev. Lett. **57**, 723 (1986).
[9] P. Fery, W. Moritz, and D. Wolf, Phys. Rev. B **38**, 7275 (1988).
[10] T. Gritsch, D. Coulman, R. J. Behm, and G. Ertl, Phys. Rev. Lett. **63**, 1086 (1989).
[11] D. G. Fedak and N. A. Gjostein, Acta Metall. **15**, 827 (1967).
[12] H. P. Bonzel and R. Ku, J. Vac. Sci. Technol. **9**, 663 (1972).
[13] P. Fery, W. Moritz, and D. Wolf, Phys. Rev. B **38**, 7275 (1988).
[14] E. C. Sowa, M. A. Van Hove, and D. L. Adams, Surf. Sci. **199**, 174 (1988).
[15] P. Fenter and T. Gustafsson, Phys. Rev. B **38**, 10197 (1988).
[16] E. Vlieg and I. K. Robinson, Surf. Sci. **233**, 248 (1990).
[17] U. Korte and G. Meyer-Ehmsen, Surf. Sci. **271**, 616 (1992).
[18] P. J. Estrup, in *Chemistry and Physics of Solid Surfaces V*, edited by R. Vanselow and R. Howe, *Springer Series of Chemical Physics* (Springer-Verlag, Berlin, 1984), p. 205.
[19] K. W. Jacobsen and J. K. Nørskov, in *The Structure of Surfaces II*, edited by J. F. van der Veen and M. A. Van Hove, *Springer Series in Surface Science*, Vol. 11 (Springer-Verlag, Berlin, 1988), p. 118.
[20] K. Christmann and G. Ertl, Z. Naturforsch. A **28**, 1144 (1973).
[21] J. L. Taylor, D. E. Ibbotson, and W. H. Weinberg, Surf. Sci. **79**, 349 (1979).
[22] M. A. Van Hove, W. H. Weinberg, and C.-M. Chan, *Low-Energy Electron Diffraction, Springer Series in Surface Science*, Vol. 6 (Springer, Berlin, 1986).
[23] W. Hetterich and W. Heiland, Surf. Sci. **210**, 129 (1989).
[24] H. Bu, M. Shi, F. Masson, and J. W. Rabalais, Surf. Sci. Lett. **230**, L140 (1990).
[25] H. Bu, M. Shi, and J. W. Rabalais, Surf. Sci. **236**, 135 (1990).
[26] W. Hetterich and W. Heiland, Surf. Sci. **258**, 307 (1991).
[27] C. Höfner, W. Hetterich, H. Niehus, and W. Heiland, Nucl. Instrum. Methods Phys. Res. B **67**, 328 (1992).
[28] W. Hetterich, U. Korte, G. Meyer-Ehmsen, and W. Heiland, Surf. Sci. Lett. **254**, L487 (1991).
[29] R. Koch, M. Borbonus, O. Haase, and K. H. Rieder, Phys. Rev. Lett. **67**, 3416 (1991).
[30] R. Koch, M. Borbonus, O. Haase, and K. H. Rieder, Appl. Phys. A: Solids Surf. **55**, 417 (1992).
[31] W. F. Avrin and R. P. Merrill, Surf. Sci. **274**, 231 (1992).
[32] J. J. Schulz, M. Sturmat, and R. Koch, Phys. Rev. B **62**, 15402 (2000).
[33] J. Kuntze, S. Speller, and W. Heiland, Surf. Sci. **402**, 764 (1998).
[34] A. Ney, J. J. Schulz, M. Sturmat, and R. Koch, Surf. Sci. **519**, 192 (2002).
[35] P. J. Feibelman, Phys. Rev. B **51**, 17867 (1995).
[36] A. Filippetti and V. Fiorentini, Phys. Rev. B **60**, 14 366 (1999).
[37] S. Ladas, S. Kennou, N. Hartmann, and R. Imbihl, Surf. Sci. **382**, 49 (1997).
[38] H. Bu, M. Shi, K. Boyd, and J. W. Rabalais, J. Chem. Phys. **95**, 2882 (1991).
[39] C.-M. Chan, K. L. Luke, M. A. Van Hove, W. H. Weinberg, and S. P. Withrow, Surf. Sci. **78**, 386 (1978).
[40] C.-M. Chan, S. L. Cunningham, K. L. Luke, W. H. Weinberg, and S. P. Withrow, Surf. Sci. **78**, 15 (1978).
[41] M. Peuckert, Surf. Sci. **144**, 451 (1984).
[42] E. Kaxiras, Y. Bar-Yam, J. D. Joannopoulos, and K. C. Pandey, Phys. Rev. B **35**, 9625 (1987).
[43] M. Scheffler, *Physics of Solid Surfaces* (Elsevier, Amsterdam, 1987).
[44] G.-X. Qian, R. M. Martin, and D. J. Chadi, Phys. Rev. B **38**, 7649 (1988).
[45] K. Reuter and M. Scheffler, Phys. Rev. B **65**, 035406 (2001).
[46] M. D. Segall, P. L. D. Lindan, M. J. Probert, C. J. Pickard, P. J. Hasnip, S. J. Clark, and M. C. Payne, J. Phys.: Condens. Matter **14**, 2717 (2002).
[47] D. Vanderbilt, Phys. Rev. B **41**, 7892 (1990).
[48] J. P. Perdew, J. A. Chevary, S. H. Vosko, K. A. Jackson, M. R. Pederson, D. J. Singh, and C. Fiolhais, Phys. Rev. B **46**, 6671 (1992).
[49] P. Blaha, K. Schwarz, G. K. H. Madsen, D. Kvasnicka, and J. Luitz, WIEN2k, an augmented plane wave+local orbitals program for calculating crystal properties, Technical University Vienna, Austria, 2001.
[50] Y. Zhang, V. Blum, and K. Reuter, Phys. Rev. B **75**, 235406 (2007).
[51] D. R. Stull and H. Prophet, *JANAF Thermochemical Tables*, 2nd ed. (U. S. National Bureau of Standards, Washington, DC, 1971).
[52] C. Kittel, *Introduction to Solid State Physics* (Wiley, New York, 2005).
[53] D. Tomanek and K. H. Bennemann, Surf. Sci. **163**, 503 (1985).
[54] I. Barin, O. Knacke, and O. Kubaschewski, *Thermochemical Properties of Inorganic Substances* (Springer-Verlag, Berlin, 1977).